3D Adaptive Multi Fracture Analysis of Composites

S. Mohammadi[1], S. Forouzan-sepehr[2]

[1] Assistant Professor, Dept. of Civil Engineering, University of Tehran, Tehran, IRAN
Homepage: http://web.ut.ac.ir/eng/cie/mohammadi, Email: smoham@ut.ac.ir
[2] PhD Student, Department of Civil Engineering, University of Tehran

Keywords: Discrete Element Method, Impact, Cracking, Composites, Delamination.

Abstract. A new approach based on the concepts of the discrete element method coupled with adaptive remeshing techniques is presented for impact resistance of composites. The method is capable of analysing progressive fracture and fragmentation behaviour as well as potential post cracking interactions caused by the newly created crack sides and segments. Anisotropic Hoffman based models are used for predicting the imminence of a material crack or interlaminar delamination. Bilinear softening models incorporating both modes I and II are also adopted to ensure mesh independency of results. A local remeshing technique is adopted every time a new crack is formed, while an overall remeshing is performed anytime a certain criterion of error estimation is violated. The special local remeshing technique is designed to geometrically model an individual crack by splitting the element, separating the failed node, creating new nodes and dividing the neighbouring elements to preserve the compatibility conditions.

Introduction

The phenomenon of failure by catastrophic crack propagation poses problems in all applications. Therefore, development of reliable models for determining the failure behaviour of growing advanced materials, such as composites, is vitally important. One of the most considerable problems in designing composite structures is their vulnerability to transverse impact, which can cause significant internal damages in terms of delamination, matrix cracking and fragmentation. In early simulations, continuum elasticity was frequently used to formulate the governing equations [1-2]. The main disadvantage of these schemes was their restriction to linear geometry of laminates [3]. More realistic models were introduced by development of contact interaction algorithms [4-6].

By introducing interface elements based on fracture mechanics, numerical simulation of crack initiation and propagation by finite elements has become more rational and popular in recent studies [7, 8]. Nevertheless, the finite element techniques, which are rooted in the concepts of continuum mechanics, are not suited to general fracture propagation and fragmentation problems. In contrast, the discrete element method (DEM), which is basically a finite element method coupled with the concepts of contact mechanics, is specifically designed to solve problems that exhibit strong discontinuities in material and geometric behaviour.

Combined FE/DE Modelling of Composites

A contact based methodology is employed for modelling and controlling of plies bonding/debonding. The interlaminar behaviours in post delamination phase, such as slipping and crack faces interactions, are also considered by contact mechanics mechanisms. In addition to 3D

contact models, a 3D anisotropic bonding model with strain softening behaviour has also been developed and implemented to investigate interlaminar crack propagation (delamination).

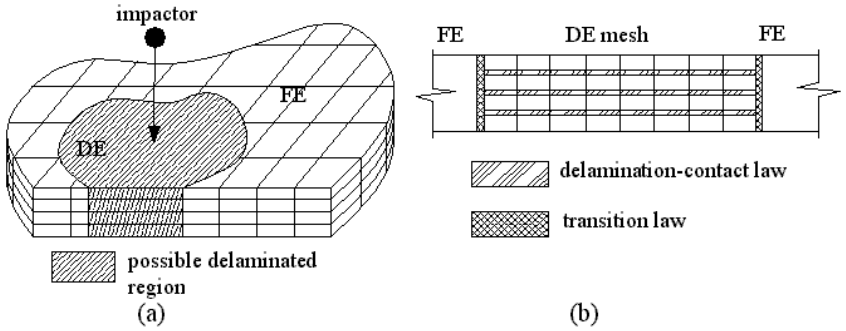

Figure 1**:** Composite specimen: (a) discrete/finite element mesh, (b) interfacial regions.

The potentially susceptible damage region of composite is modelled using discrete element mesh and the rest of the specimen is modelled with coarser solid elements to reduce the analysis time (Fig. 1(a)). Each discrete element is discretized by a finite element mesh; finer mesh for the plies closer to the impact region and coarser mesh for the furthest ones. The interlaminar characteristics of plies such as debonding, impenetrability, friction and sliding determine connection (bonding) states of the adjacent discrete elements (Fig. 1(b)). Discrete element system and finite element mesh of the rest of the shell are connected together by transition interface, preventing debonding under all stress conditions. Non-linear material properties (using Hoffman anisotropic yield criterion) and geometric nonlinearities (large deformation) are also considered in the FE formulation [9].

Contact Constitutive Relationship

A bilinear strain-softening model [10] together with the penalty method to impose impenetrability and frictional contact are employed. A contact gap vector can be described as

$$\mathbf{g} = [g_N , \mathbf{g}_T]^{\mathrm{T}} \tag{1}$$

where g_N is the normal distance between contactor node and contact segment. $\mathbf{g}_T$ is a tangential vector whose size is equal to the distance between the projection of the contact node in the current configuration and the initial configuration.

Combining the bilinear strain-softening model with the penalty method leads to constitutive interfacial relationship in pure modes I and II (Fig. 2), where g_T is the magnitude of vector $\mathbf{g}_T$, $\bar{\sigma}_N$ and $\bar{\sigma}_T$ are the threshold tensile and shear strength of the binder between plies while $\bar{g}_0^N$ and $\bar{g}_0^T$ are the related displacements. $\bar{g}_{\max}^N$ and $\bar{g}_{\max}^T$ are the maximum normal and tangential displacements, which the binder can bear without debonding. $G_{c\,\mathrm{I}}$ and $G_{c\,\mathrm{II}}$ are assumed to be material constants of fracture energy release rate for modes I and II defined by [3]

$$G_{c\,\mathrm{I}} = \tfrac{1}{2}\bar{\sigma}_N \, \bar{g}_{\max}^N \quad , \quad G_{c\,\mathrm{II}} = \tfrac{1}{2}\bar{\sigma}_T \, \bar{g}_{\max}^T \tag{2), (3}$$

and $\bar{\sigma}_N$ and $\bar{\sigma}_T$ can be obtained by experiments. α_N and α_T are the penalty parameters, and

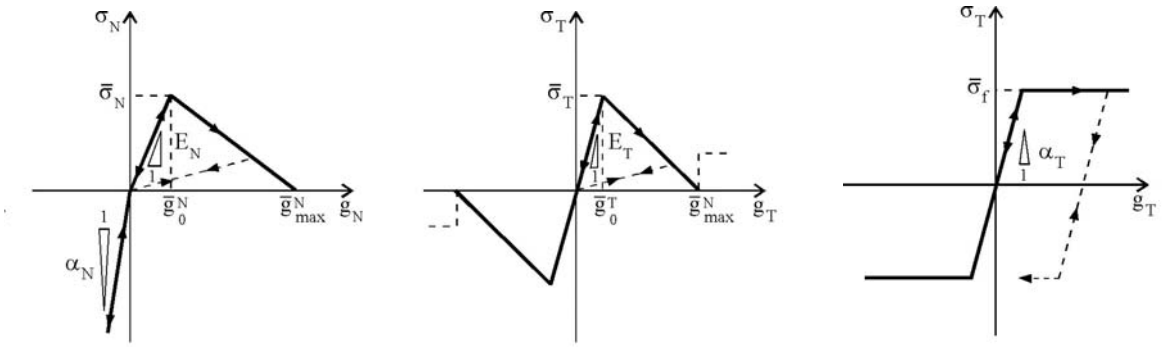

(a) (b) (c)

Figure 2: Normal and tangential contact stress—gap vector magnitude diagram: (a) pure normal mode, (b) pure tangential mode in adhesion phase, (c) pure tangential mode in friction phase

$$\bar{\sigma}_f = \mu\langle -\sigma_N \rangle \tag{4}$$

where μ is the Coulomb coefficient of dry friction and $\langle \bullet \rangle$ denotes the Macaulay function, that is

$$\langle x-a \rangle = \begin{cases} x-a & ; x \geq a \\ 0 & ; x < a \end{cases} \tag{5}$$

Figure 2 shows the stress-displacement relationship in pure modes I and II. Here, the concept of extenet of delamination damage introduced by [10] has been employed:

$$\kappa = \sqrt{\left\langle \frac{g_N}{\bar{g}_0^N} \right\rangle^2 + \left(\frac{g_T}{\bar{g}_0^T} \right)^2} - 1 \tag{6}$$

According to this model, delamination will initiate as soon as κ exceeds zero. Combination of this model and the Penalty method leads to the constitutive relationship between interfacial stresses and their related displacements, that is

$$\boldsymbol{\sigma}^{\mathrm{c}} = \begin{bmatrix} \sigma_N & \boldsymbol{\sigma}_T \end{bmatrix}^{\mathrm{T}} = \mathbf{D}^{\mathrm{c}}\,\mathbf{g} \quad , \quad \mathbf{D}^{\mathrm{c}} = \mathrm{Diag}\left[D_N^{\mathrm{c}}(\mathbf{g}), D_T^{\mathrm{c}}(\mathbf{g}), D_T^{\mathrm{c}}(\mathbf{g}) \right] \tag{7), (8}$$

Defining three parameters $S_N(\kappa)$, $S_T(\kappa)$ and g_{Tu}^* as

$$S_N(\kappa) = \frac{\kappa}{1+\kappa} \cdot \frac{\bar{g}_{\max}^N}{\bar{g}_{\max}^N - \bar{g}_0^N} \quad , \quad S_T(\kappa) = \frac{\kappa}{1+\kappa} \cdot \frac{\bar{g}_{\max}^T}{\bar{g}_{\max}^T - \bar{g}_0^T} \tag{9), (10}$$

$$g_{Tu}^* = \bar{g}_0^T \sqrt{\left\langle \left(\frac{\bar{g}_{\max}^T}{\bar{g}_0^T} \right)^2 - \left\langle \frac{g_N}{\bar{g}_0^N} \right\rangle^2 \right\rangle} \tag{11}$$

results in

$$D_N^{\mathrm{c}}(\mathbf{g}) = \begin{cases} \alpha_N & ; \quad g_N \leq 0 \\ E_N & ; \quad g_N > 0 \,,\, \kappa \leq 0 \\ \left(1 - S_N(\kappa)\right) E_N & ; \quad g_N > 0 \,,\, S_N(\kappa) < 1 \\ 0 & ; \quad g_N > 0 \,,\, S_N(\kappa) \geq 1 \end{cases} \tag{12}$$

$$D_T^{\mathrm{c}}(\mathbf{g}) = \begin{cases} E_T & ; \quad \kappa \le 0 \\ \left(1 - S_T(\kappa)\right) E_T & ; \quad \kappa > 0 \,,\, S_T(\kappa) < 1 \\ \left(\dfrac{g_{Tu}^*}{g_T} - 1 \right) \alpha_T & ; \quad S_T(\kappa) \ge 1 \,,\, g_T < g_{Tu}^* + \dfrac{\overline{\sigma}_f}{\alpha_T} \\ \dfrac{\overline{\sigma}_f}{g_T} & ; \quad S_T(\kappa) \ge 1 \,,\, g_T \ge g_{Tu}^* + \dfrac{\overline{\sigma}_f}{\alpha_T} \end{cases} \tag{13}$$

Error Estimation and Transfer Techniques

A Zienkiewicz-Zhu error estimator [12] is used to anticipate the error distribution throughout the damaged composite model. Any time the overall error violates a certain criteria, the global remeshing is performed. One of the main concerns is to adopt a reliable transfer technique for transferring the state variables and history data from the old mesh to the new one.

In elastic-plastic problems, there exist two basic types of variables to be transferred, i.e., nodal values such as displacements and velocity, and quantities associated to the quadrature points such as internal energy density, the equivalent plastic strain, plastic strain tensor. Here, the methodology proposed by Peric[13] and Dutko [14] is adopted, where two separate but compatible transfer operators, namely τ_1 and τ_2 for Gauss point and nodal variables, respectively, are defined.

For simplicity of notation, the state array $\Lambda(h,n) = \widetilde{\Lambda}(h,n) \bigcup \hat{\Lambda}(h,n)$ is defined, which contains all nodal, $\hat{\Lambda}(h,n)$, and Gauss point, $\widetilde{\Lambda}(h,n)$, information at a given time step t_n and mesh h. When the estimated error of the solution $\Lambda(h,n)$ violates a prescribed criterion at time t, a new mesh, h+1, is generated and a new solution $\Lambda(h+1,n+1)$ is computed.

The transfer operator τ_1

The process comprises three distinct steps, i.e., projection of the Gauss point variables to nodes, transfer of the nodal values from the old to the new mesh and projection of the corresponding nodal quantities to new quadrature points.

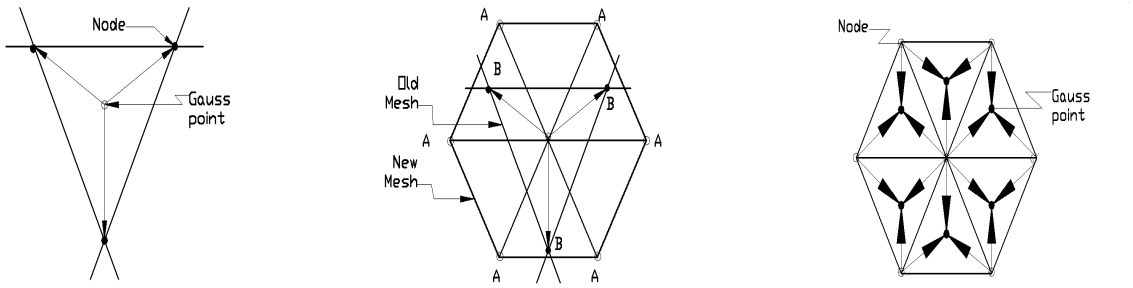

a) Projection of variables to nodes b) Transfer from old to new mesh c) Nodes to Gauss point interpolation

Figure 3– Transferring Gauss point variables from old to the new mesh.

(a) Projecting Gauss point variables to nodes

The transfer of Gauss point variables to nodes is performed using the well-known projection/smoothing technique, largely used for error estimates and based on Zienkiewicz and Zhu's [12] approach. Fig. 3(a) illustrates the operation for constant strain triangles, where the subscripts N and G indicate nodal and Gauss point variables, respectively.

(b) Transferring the nodal projection to the new mesh

The second step (Fig. 3(b)) is the most complex, in which the projection/smoothed components of the state array, $\widetilde{\Lambda}^*(h,n,N)$, are transferred from old mesh h to the new mesh h+1. The process can be subdivided into three stages. In the first stage, for every node A of the new mesh h+1 with coordinates ${}^{h+1}x_{n,A}$, a background element, ${}^{h}\Omega^{e}$, is found in the old mesh for which ${}^{h+1}x_{n,A} \in {}^{h}\Omega^{e}$. The second stage constitutes the evaluation of the local coordinates, $({}^{h}\xi_A, {}^{h}\eta_A)$, of the node A of the new mesh within the background element by solving

$$ {}^{h+1}x_{n,A} = \sum_{b=1}^{r} {}^{h}N_b({}^{h}\xi_A, {}^{h}\eta_A)\, {}^{h}x_{n,b} \tag{14} $$

where r is the number of nodes of element and N is the interpolation function. In the third stage, the state variables $\widetilde{\Lambda}(h+1,n,N)$ are mapped from nodes B of the old mesh to nodes A of the new mesh h+1 by using the interpolation function ${}^{h}N_b({}^{h}\xi_A, {}^{h}\eta_A)$ as

$$ \widetilde{\Lambda}(h+1,n,A) = \sum_{b=1}^{r} {}^{h}N_b({}^{h}\xi_A, {}^{h}\eta_A)\, \widetilde{\Lambda}^*(h,n,b) \tag{15} $$

(c) Interpolating Gauss point variable in the new mesh

In the final step, which is illustrated in Fig. 3(c), Gauss point variables $\widetilde{\Lambda}(h+1,n,G)$ of the new mesh are obtained by using the interpolation function of the element ${}^{h+1}\Omega^{(e)}$ as

$$ \widetilde{\Lambda}(h+1,n,G) = \sum_{a=1}^{r} {}^{h+1}N_a({}^{h+1}\xi_G, {}^{h+1}\eta_G)\, \widetilde{\Lambda}\,(h+1,n,a) \tag{16} $$

in which $({}^{h+1}\xi_G, {}^{h+1}\eta_G)$ are the Gauss point coordinates.

The transfer operator τ_2

The present task reproduces the mapping of the nodal values operation as

$$ \hat{\Lambda}(h+1,n,A) = \sum_{b=1}^{r} {}^{h}N_b({}^{h}\xi_A, {}^{h}\eta_A)\, \hat{\Lambda}(h,n,b) \tag{17} $$

Numerical Simulations of Buckling of a Delaminated Composite Panel

A $[0_{20}]$ composite panel with an initial interlaminar crack between the $0_4/0_{16}$ layers is subjected to compressive loading as depicted in Fig. 4. The loading incrementally increases until the local and global buckling modes occur in 0_4 and 0_{16} layers, respectively. Fig. 5 shows the predicted local and global buckling modes. According to Fig. 5, local buckling commenced at load 1410 (lbf/in) and global buckling occurred at load 7130 (lbf/in), comparable to the results reported by Progini [15] at 1312 (lbf/in) and 7821 (lbf/in), respectively.

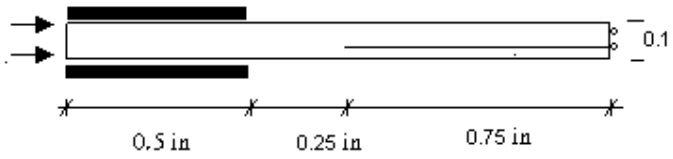

Material Properties of Composite Panel	
E_{xx}= 20200 ksi	E_{yy}=1410 ksi
E_{zz}=1410 ksi	G_{xy}=810 ksi
G_{yz}=546 ksi	ν_{xy}=0.29
ν_{xz}=0.29	ν_{yz}=0.29
X_T=220 ksi	X_C=231 ksi
Y_T=6.46 ksi	Y_C=36.7 ksi
S = 15.5 ksi	G_{IC}=0.5 lbf/in
G_{IIC}=0.5 lbf/in	

Figure 4. Geometry and properties of a composite panel with an initial interlaminar crack.

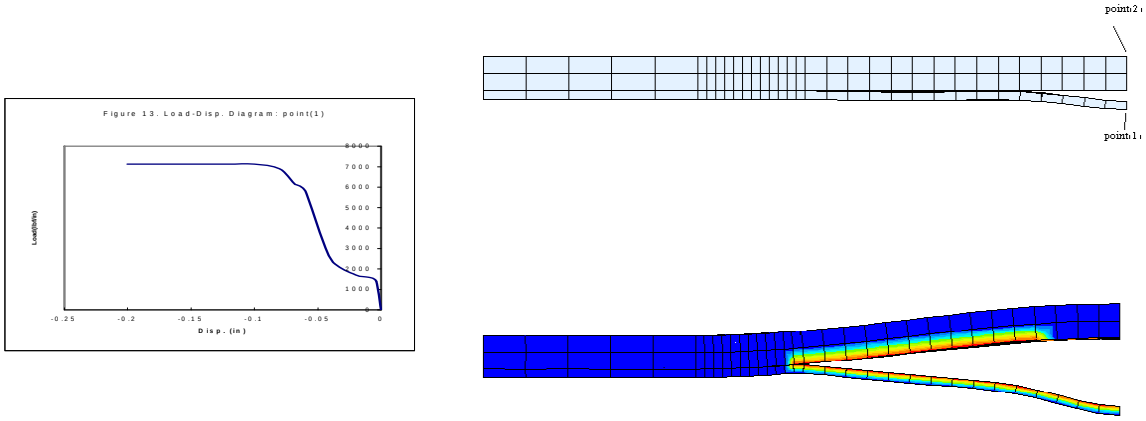

Figure 5. Local and global buckling modes.

High Velocity Impact on a Composite Plate

An experimental composite specimen [16] subjected to a triangular load applied from 0 to 5 μsec with a peak force of 5kN is considered (Fig. 6). More than 30000 unstructured pentahedral elements and 25000 nodes were initially used for adaptive fracture modelling of the plate. The fracture and delamination patterns of the plate at $t = 0.0245$ sec are illustrated in Fig. 7. The shaded areas represent the failed region at different layers.

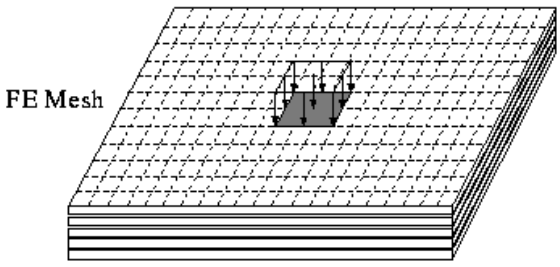

Model size = $0.1524 \times 0.1524 \times 0.00444$ m

Ply region = $[+45_n, -45_n, +45_n, -45_n, +45_n]$

$E_{xx} = 152.4\text{E}3$ MPa	$E_{yy} = 10.7\text{E}3$ MPa
$\nu = 0.35$	$\rho = 0.35\ \text{kg}/\text{m}^3$
$X_t = 2772$ MPa	$X_c = 3100$ MPa
$Y_t = 79.3$ MPa	$Y_c = 231.0$ MPa
$S = 132.8$ MPa	

Figure 6: FE/DE mesh of the composite specimen

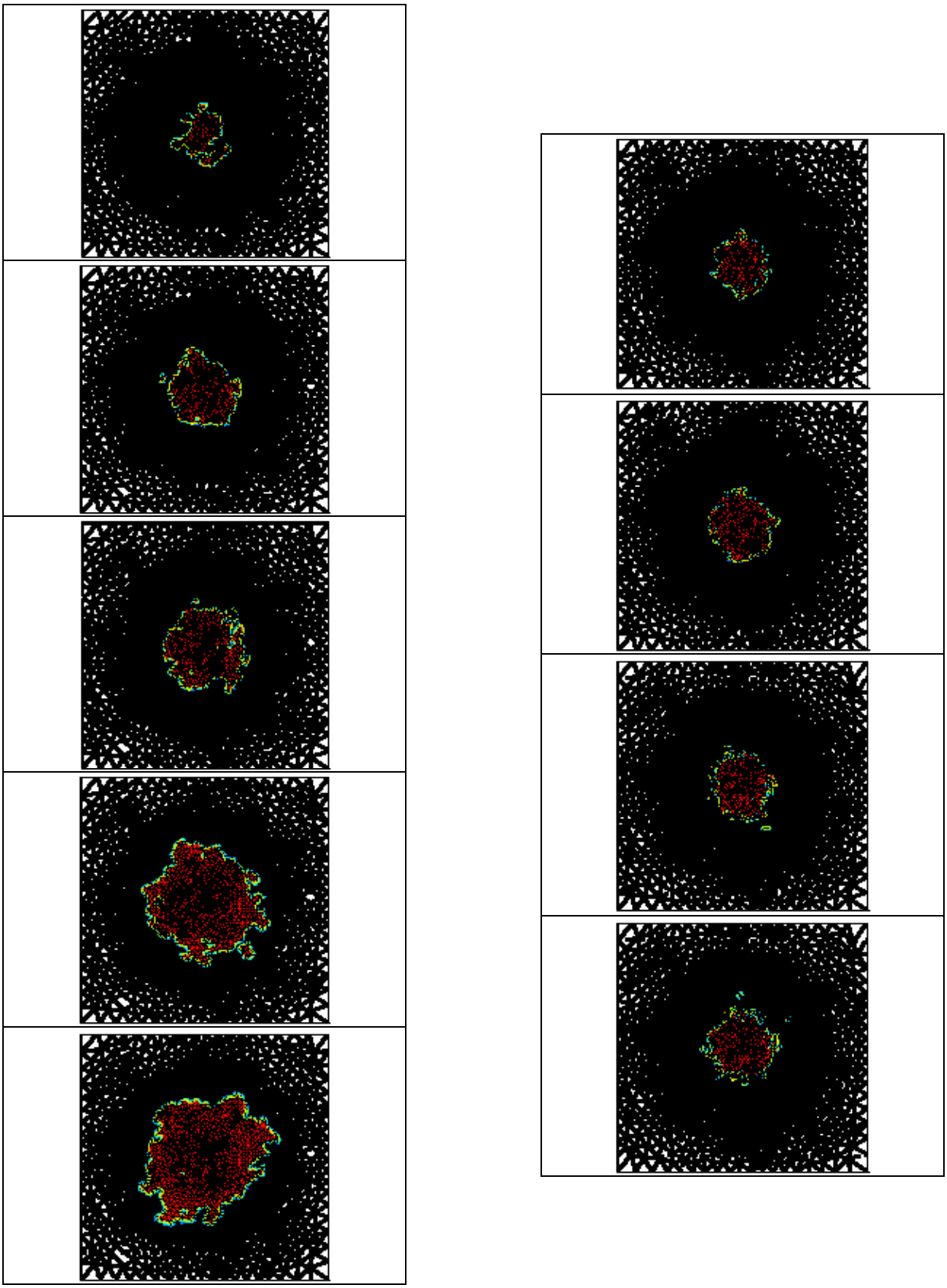

Figure 7: Fracture and delamination patterns at different layers/interfaces of the composite mesh.

Conclusions

A combined adaptive finite/discrete element method has been successfully developed for 3D damage analysis of composites. The initiation and propagation of cracks have been considered by using a bilinear strain-softening model. The penalty method has been employed to impose impenetrability and post-debonding behaviours of plies as well as post-cracking of individual layers. Numerical tests have been used to assess the performance of the method, showing the power of the algorithm for numerical simulation of impact loading on composite structures. The method is expected to perform well for similar applications which exhibit progressive fracturing.

Acknowledgements
The authors would like to acknowledge the support received from the "University of Tehran, Vice Chancellor for Research" under the grant number 614/2/627.

References:

[1] O'Brien (1985); "Analysis of local delaminations and their influence on composite laminate behaviour", Delamination and Debonding of Materials, ASTM STP 876, 282-297.

[2] R.E. Rowlands (1985); "Strength (failure) theories and their experimental correlation", Handbook of Composites, vol. 3—Failure Mechanics of Composites, Elsevier, Amsterdam, Ch. 2, 71-125.

[3] S. Mohammadi, D.R.J. Owen, D. Perić (1998); "A combined finite/discrete element algorithm for delamination analysis of composites", *Finite Elements in Analysis and Design*, **28**, 321-336.

[4] W.H. Chen, S.H. Yang (1996); "Multilayer hybrid-stress finite element analysis of composite laminates with delamination cracks origination from transverse cracking", *Engineering Fracture Mechanics*, **54** (5): 713-729.

[5] Y.W. Kwon, H. Aygunes (1996); "Dynamic finite element analysis of laminated beams with delamination cracks using contact-impact conditions", *Computers & Structures*, **58** (6): 1161-1169.

[6] G.E. Stravroulakis, P.D. Panagiotopoulos (1985); "On the interface debonding and frictional sliding in composites: the material inclusion problem", Delamination and Debonding of Materials, 165-172.

[7] F. Hashagen, R. de Borst (2000); "Numerical assessment of delamination in fibre metal laminates", *Computer Methods in Applied Mechanics and Engineering*, **185**, 141-159.

[8] W. Sprenger, F. Gruttmann, W. Wagner (2000); "Delamination growth analysis in laminated structures with continuum-based 3D-shell elements and a viscoplastic softening model", *Computer Methods in Applied Mechanics and Engineering*, **185**, 123-139.

[9] S. Mohammadi, D.R.J. Owen, D. Perić (2000); "3D Progressive Damage Analysis of Composites by Combined Finite/Discrete Element Approach", ECCOMAS 2000, Barcelona, Published on CD.

[10] Y. Mi, M.A. Crisfield, G.A.O. Davies, H.B. Hellweg (1998); "Progressive delamination using interface elements", *J. Composite Materials*, **32:14**, 1246-1272.

[11] S. Mohammadi, S. Forouzan-sepehr, A. Asadollahi (2002)); "Contact based delamination and fracture analysis of composites", *Thin-Walled Structures*, **40**, 595-609.

[12] O. C. Zienkiewicz, J. Z. Zhu, A simple error estimator and adaptive procedure for practical engineering analysis, Int. J. Num. Meth. Eng. **24** (1987) 337-357.

[13] D. Peric, C. Hochard, M. Dutko, D. R. J. Owen, Transfer operators for evolving meshes in small strain elasto- plasticty, Comp. Mech. Appl. Mech. Eng. **137** (1996) 331-344.

[14] M. Dutko, D. Peric, D. R. J. Owen, Z. Wei, J. Yu, Bulk forming simulation by adaptive explicit FEM, Computational Plasticity, CIMNE, (1997) 1305-1312.

[15] P. Progini, A. Riccio, F. Scaramuzzino, "Influence of Delamination Growth and Contact Phenomena on the Compressive Behavior of Composite Panels", Journal of Composite Materials, Vol.33, No. 15, pp.1433-1465, 1999

[16] M.J. Worswick, P.V. Strazincky, O. Majeed (1995); "Dynamic fracture of fibre reinforced composite coupons", Dynamic Response and Behaviour of Composites, ASME AD: **46**, 29-41.